TCAD Analysis of Leakage Currents in the Ballistic Regime

P. Aguirre, S. Sant, and A. Schenk

Integrated Systems Laboratory, ETH Zurich, Gloriastrasse 35, CH-8092 Zurich, Switzerland
adelia@iis.ee.ethz.ch

Introduction: In this work it is demonstrated how ballistic mobility (μ_b) models [1,2] affect the leakage currents in ultra-short FETs using a semi-classical device simulator [3,4]. **Method:** The test device and relevant parameters are shown in Fig. 1. Ballistic I_D-V_{GS} characteristics obtained from the quantum-transport tool QTx [5] served as reference. Source-to-drain tunneling (STDT) which dominates the sub-threshold current at ultra-short gate lengths [6] was simulated by the default "Non Local Tunneling" (NLT) model implemented in [4]. Two μ_b-models where used to better match the ON-current (I_{ON}) with the QTx reference. The first has a ballistic electron velocity (v_b) dependent on the quasi-Fermi potential (QFP) ψ_n [1,2]. In the second, v_b is a function of the electron density n_{TOB} at the top of the source-to-drain potential barrier [1]. A leakage mechanism inherent in DG transistors and FinFETs is the floating-body effect (FBE) [7] caused by band-to-band tunneling (BTBT) and affected by Shockley-Read-Hall (SRH) recombination. Models available in [4] were used in the TCAD simulations.

Results: Fig. 2a shows that the $v_b(n_{TOB})$-model can well reproduce the quantum-ballistic I_{ON}, but the sub-threshold current becomes corrupted. This can be traced back to the deformation of $\psi_n(x)$ (see Fig. 2b). As the STDT rate of the NLT model is computed with the local QFPs at the classical turning points (x_t) for each tunnel path, the deformed $\psi_n(x)$ artificially suppresses the tunnel current. The red curve in Fig. 3 was obtained by a post-processing calculation of the STDT current using the contact Fermi levels in the NLT model instead of $\psi_n(x_t)$. This removes the artifact in the deep sub-threshold range (first two points), but quickly leads to deviations from the self-consistent TCAD solution which contains the ordinary drift-diffusion current. The ballistic velocity models also impact the BTBT rates which locally depend on the QFPs (see Fig. 5a). The transfer curves in Fig. 4 (with BTBT+SRH added to STDT) exhibit the additional FBE-induced leakage current. The stronger sensitivity of the BTBT rate to the $v_b(n_{TOB})$-model as compared to the $v_b(\psi_n)$-model can be traced back to a stronger deformation of $\psi_n(x)$ in the channel-drain junction where the electron BTBT rate is maximal (Fig. 5b). The relative effect is not much changed even at an extreme rate of ~10^{32} cm^{-3}s^{-1} (see Fig. 6).

[1] P. Aguirre et al., Solid-States-Electronics, accepted, 2019. [2] O. Penzin et al., IEEE T-ED **64,** 2017. [3] M. Ieong et al., IEDM, 1998. [4] Synopsys Inc., Sentaurus Device User Guide, V-2016.03, 2016. [5] M. Luisier et al., Jour. Appl. Phys. **100**(4), 043713, (2006). [6] F. Heinz et al., Jour. Appl. Phys. **100**(8), 084314, 2006. [7] S. Sant et al., IEEE T-ED **65** (6), 2578-2584, 2018.

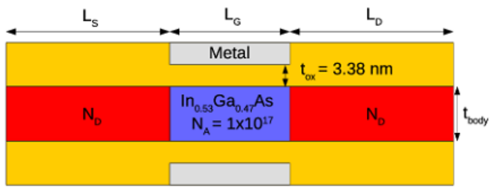

Fig.1: Schematic of an $In_{0.53}Ga_{0.47}As$ double-gate (DG) ultra-thin-body FET. Parameters: $N_D = 5 \times 10^{19}$ cm^{-3}, $L_S = 20$ nm, $L_G = 11.5$ nm, $t_{body} = 4.2$ nm, and $m_e = 0.0678\, m_0$.

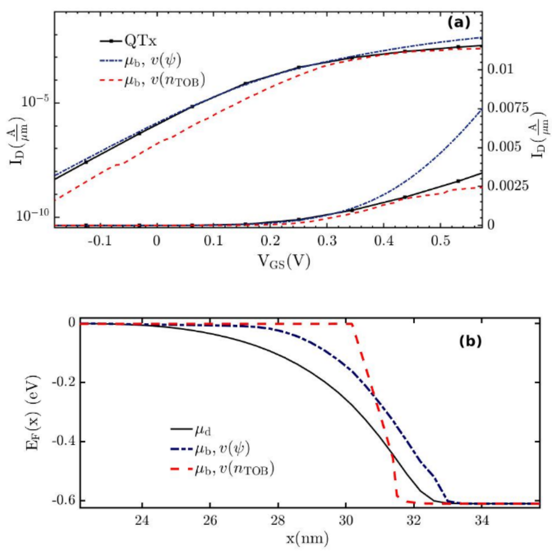

Fig.2: (a) I_D-V_{GS} characteristics at $V_{DS} = 0.61$ V of the device depicted in Fig. 1 with a tunnel mass $m_t = m_e$. (b) Fermi energy profiles $-e\psi_n(x)$ for different electron mobilities ($\mu_d = 1 \times 10^3$ cm^2/Vs, $\mu_b[v(\psi_n)]$, and $\mu_b[v(n_{TOB})]$), all extracted at $V_{GS} = -0.2$ V and $V_{DS} = 0.61$ V.

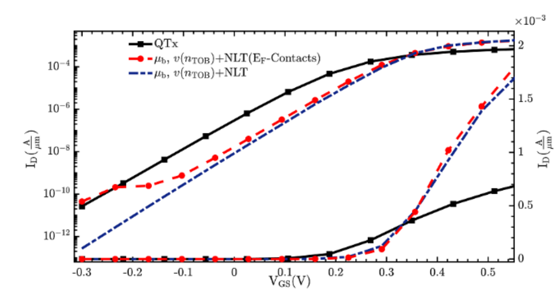

Fig.3: I_D-V_{GS} characteristics at $V_{DS} = 50$ mV of the device depicted in Fig. 1 with a tunnel mass $m_t = m_e$. The red curve was obtained by a post-processing calculation of the STDT current using the contact Fermi energies in the NLT model instead of local QFPs.

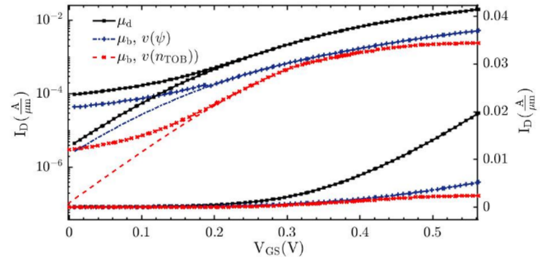

Fig.4: I_D-V_{GS} characteristics at $V_{DS} = 1$ V of the device depicted in Fig. 1 for different electron mobilities ($\mu_d = 1 \times 10^3$ cm^2/Vs, $\mu_b[v(\psi_n)]$, and $\mu_b[v(n_{TOB})]$) with $m_e = 0.0678\, m_0$, $m_h = 0.446\, m_0$, and SRH lifetimes $\tau_e = \tau_h = 1$ ns. The actual band gap of $E_G = 1.7$ eV caused by the strong confinement was lowered to $E_G = 0.7$ eV in order to enhance the effect of BTBT. Curves without BTBT are shown for comparison (dashed and dot-dashed lines).

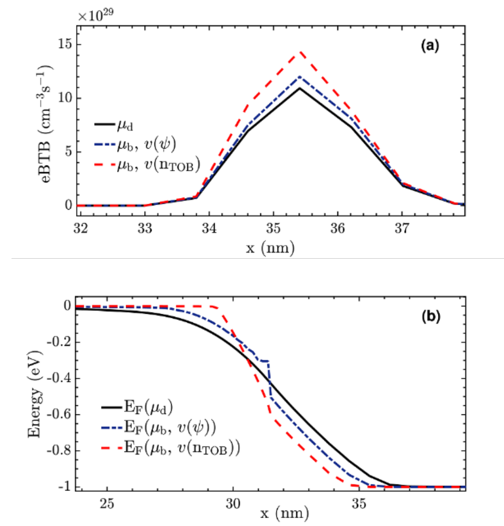

Fig.5: (a) Electron BTBT rates for different electron mobilities ($\mu_d = 1 \times 10^3$ cm^2/Vs, $\mu_b[v(\psi_n)]$, and $\mu_b[v(n_{TOB})]$) extracted at $V_{GS} = 0$ V and $V_{DS} = 1$ V. Parameters are the same as in Fig. 4. (b) Corresponding profiles of the electron Fermi energy $-e\psi_n(x)$.

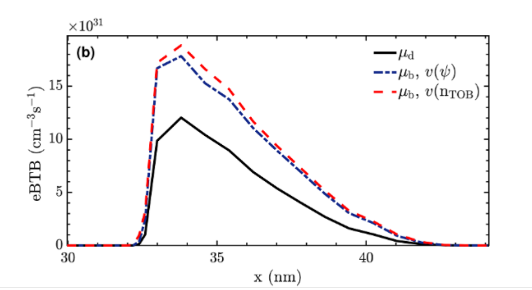

Fig.6: Electron BTBT rates for different electron mobilities ($\mu_d = 1 \times 10^3$ cm^2/Vs, $\mu_b[v(\psi_n)]$, and $\mu_b[v(n_{TOB})]$) extracted at $V_{GS} = 0$ V and $V_{DS} = 2.5$ V.